THE JOURNAL OF PHYSICAL CHEMISTRY B

Article

pubs.acs.org/JPCB

Influence of the Water Content on the Structure and Physicochemical Properties of an Ionic Liquid and Its Li^+ Mixture

Vitor L. Martins,[†] Bruno G. Nicolau,[†,§] Sérgio M. Urahata,[‡] Mauro C. C. Ribeiro,[†] and Roberto M. Torresi*,[†]

[†]Instituto de Química and [‡]Instituto de Física, Universidade de São Paulo (USP), CP 26077, 05513-970 São Paulo-SP, Brazil

Supporting Information

ABSTRACT: The effect of water on the hydrophobic ionic liquid (IL) 1-*n*-butyl-2,3-dimethylimidazolium bis-(trifluoromethanesulfonylimide) and its Li^+ mixture was evaluated. The electrochemical stability, density, viscosity, and ionic conductivity were measured for both systems in different concentrations of water. The presence of Li^+ causes a large increase in the water absorption ability of the IL. The experimental results suggest a break of the interactions between Li^+ and Tf_2N^- anions in the strong aggregates formed in dried Li^+ mixtures, modifying the size and physicochemical nature of these aggregates. It is also observed that the size of the ions aggregates with formal charge increases at high temperature and decreases the mobility of the charge carrier, explaining the break in the Walden rules at high temperature. Raman spectroscopy and molecular dynamic simulations show the structural change of these systems. In neat ILs, the water molecules interact mainly among each other, while in the Li^+ mixtures, water interacts preferentially with the metallic cation, causing an important change in the aggregates present in this system.

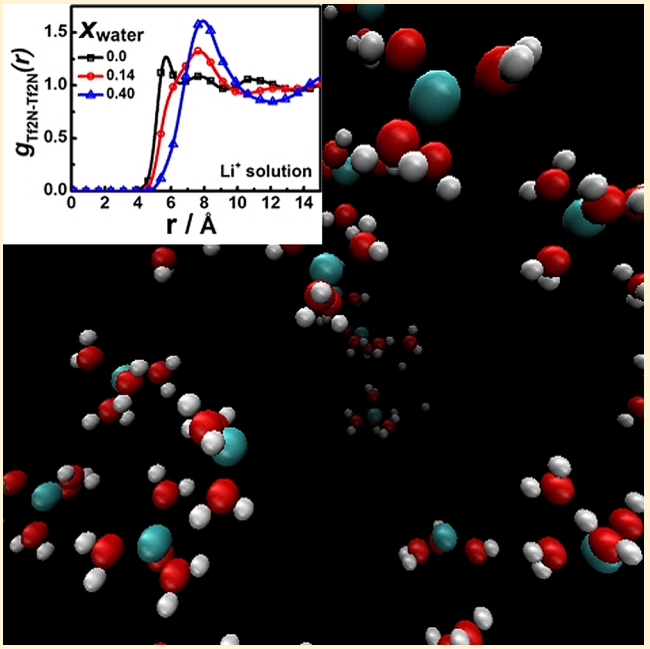

1. INTRODUCTION

Ionic liquids (ILs) have been studied by many research groups because they can be applied in many fields, such as catalysis,[1−4] synthesis,[5,6] electrodeposition,[7−10] and as the electrolyte in rechargeable batteries.[11−15] Some of the properties that make ILs good as electrolytes in electrochemical systems are their intrinsic ionic conductivity, their large electrochemical window, and their high thermal and chemical stability.[16] In addition to these properties, there are other interesting characteristics of ILs that make them an object of vast study, such as the possibility of tuning the IL properties by modifying one part of some component; changing the side chain[17] or even the cyclic component of the cation[18] can improve some properties of the IL, for example increasing the transport properties or the chemical and electrochemical stability.

Research groups are in accordance that small quantities of impurities can cause a large change in the IL properties,[19] which may be the reason for the nonreproducibility of results among different groups[20−22] for the same IL. Previous works have reported studies of mixtures of a hydrophilic IL and water, focusing on physical properties.[23−25] Other works have approached the structure of these mixtures by molecular dynamics (MD) simulation, showing the nanoconfinement of water because, in high water concentrations, the saturation of H-bonds among water and anions is reached, favoring the H-bond between water molecules.[26] Furthermore, the modification of the cation side chain plays a significant role in the cation aggregation in the presence of water.[27] Mixtures of an imidazolium-based IL with a hydrophilic anion and water have been studied mainly due the self-organization and micelle formation of the cation in the presence of water,[28] mainly when the cation presents a long side chain, which interacts with others to form micelles. By exchanging the anion for a hydrophobic one, the structure becomes nonmicellar, and phase separation occurs.[29] Due to these interesting effects, hydrophilic ILs have received more attention in these studies.[27] The water effect in the structure of three ILs was reported recently, indicating the formation of clusters and the break of the interactions between ions, and the authors claimed that for a mixture with 70 mol % or more of water, the system turned

Received: December 29, 2012
Revised: July 1, 2013
Published: July 1, 2013

   dx.doi.org/10.1021/jp312839z | *J. Phys. Chem. B* 2013, 117, 8782−8792

out to be an aqueous solution.[30] Others reports have evaluated the dynamics properties of water and benzene in ILs by MD simulations and NMR techniques,[31,32] showing that rotational diffusion explains the major portion of the spectral density.

The use of ILs in Li ion or Li rechargeable batteries requires the study of mixtures of ILs and Li^+ salt[13,33] because the anode material must show Li^+ intercalation/deintercalation or Li deposition/dissolution and the cathode material must demonstrate Li^+ intercalation/deintercalation.[34−38] Many research groups have reported studies regarding the physicochemical properties[13,16,39−45] and the local structure[46−54] of these mixtures in terms of the application to secondary batteries.

The effect of water as an impurity on some physicochemical properties such as the viscosity,[21,55−57] the ionic conductivity,[58] and the electrochemical stability[59] has been already reported for some neat hydrophobic ILs. Therefore, considering the results already reported, in addition to the effect of water on some properties of the neat IL 1-*n*-butyl-2,3-dimethylimidazolium bis(trifluoromethanesulfonylimide) ([BMMI][Tf_2N]), this study also addresses the influence of water on the $LiTf_2N$ mixture in [BMMI][Tf_2N] in terms of physicochemical properties, such as the density, viscosity, ionic conductivity, and electrochemical window. Raman spectroscopy and MD simulations were used to provide insights into the microscopic nature of the ionic aggregates and to compare the influence of water on these properties for both systems to relate the physicochemical properties with changes in the liquid structure.

2. EXPERIMENTAL METHODS

The Li^+ mixture was obtained by mixing the proper amount of $LiTf_2N$ (Aldrich) in [BMMI][Tf_2N] (IOLITEC). The resulting mixture had a molar fraction of 0.16 Li^+, that is, the empirical formula of this mixture is $[Li]_{0.33}[BMMI]_{0.67}[Tf_2N]$. In the following, [BMMI][Tf_2N] and [Li][BMMI][Tf_2N] will be called, respectively, the neat IL and Li^+ mixtures, even in the presence of water. After purchase, the IL was moved to an argon atmosphere glovebox Labmaster 130, with H_2O and O_2 concentrations below 1 ppm. Two methods to add water to the neat IL and Li^+ mixtures were used. In mixtures with a low concentration of water, the mixture was maintained under mechanical stirring in an open system until it reached the required concentration of water. In mixtures with a high concentration of water, deionized water was added with the assistance of a micropipet. These two steps were performed outside of the glovebox, and after that, these mixtures were sealed and stored in the glovebox. The amount of water was measured by coulometric titration by a Karl Fischer method (756 KF, Metrohm). The driest samples give the amount of water from the chemicals as received; the neat IL had 55.80 ppm (0.0040 mol L^{-1}) of water, and the Li^+ mixture had 120.0 ppm (0.010 mol L^{-1}) of water.

Viscosity and density measurements were conducted in a Viscosimeter SVM 3000 (Anton Paar) in a temperature range from 4.7 to 71.8 °C. The ionic conductivity was measured by electrochemical impedance spectroscopy with Autolab PGSTAT 30 (Eco Chemie) equipment in the frequency range of 0.01 and 10 kHz. The cell constant was calibrated with a KCl standard aqueous solution. The ionic conductivity cell was set up inside of the glovebox, and the measurements were made outside by varying the temperature with the assistance of a thermostatic bath (Lauda E106) in the same range of viscosity measurements.

Raman spectra at room temperature were obtained with a FT-Raman RFS 100 Bruker excited with a 1064 nm Nd:YAG laser with an output power of 400 mW and a resolution of 1 cm^{-1}. Higher-temperature spectra were obtained with a Jobin-Yvon U-1000 Raman spectrometer excited with the 647.1 nm line of a Kr^+ ion laser with an output power of 400 mW and a resolution of 0.34 cm^{-1}.

The electrochemical window was determined by linear sweep voltammetry using Autolab PGSTAT 30 (Eco Chemie) equipment with a glassy carbon disk as the working electrode and a Pt mesh and wire as the counter and reference electrodes, respectively, at 10 mV s^{-1} starting from the open-circuit potential. The limits were arbitrarily defined as the potential at the current density reached ±150 μA cm^{-2}.

3. COMPUTATIONAL DETAILS

The MD simulations were performed with a potential energy function considering the intermolecular Lennard-Jones and Coulombic interactions, and the intramolecular interactions considered the bond stretching, r, the angle bending, θ, and the torsion of the dihedral angles, ψ

$$V_{total} = \sum_{i,j;i<j} \left\{ 4\epsilon_{ij} \left[\left(\frac{\sigma}{r_{ij}} \right)^{12} - \left(\frac{\sigma}{r_{ij}} \right)^{6} \right] + \frac{q_i q_j}{r_{ij}} \right\} + \sum_{bonds} k_b (r - r_{eq})^2 + \sum_{angles} k_\theta (\theta - \theta_{eq})^2 + \sum_{dihedrals} k_\psi [1 + \cos(n\psi - \delta)] \quad (1)$$

where r_{ij} is the distance between atoms i and j of different ions. Parameters such as the bond lengths, r_{eq}, the angles, θ_{eq}, the dihedral angles, ψ_{eq}, and the force constant parameters are based on the all-atoms models of Morrow et al.[60] and Monteiro et al.[46] for the $BMMI^+$ cation (hydrogen is not explicit) and those of Lopes et al.[61] and Borodin et al.[62] for the Tf_2N^- anion, and Li^+ paramenters were taken from Monteiro et al.[46] The SPC/Fw water model[63] was used to simulate wet systems. The simulations were conducted in a cubic box generated by Packmol[64] with a random configuration at 400 K to achieve significant ionic mobility and a proper statistical average; the number of molecules in each system is presented in Table 1S (Supporting Information). Pre-equilibrium simulations were conducted, allowing the variation of the box size using the Berendsen's barostat to reach the average pressure of 0.1 MPa and the expected density for this temperature. The equilibration runs were longer than 2.0 ns with a time step of 3.0 fs. The production runs were longer than 5.0 ns with a time step of 3.0 fs in a *NVE* ensemble with an equation of motion integrated with the velocity Verlet algorithm[65] as the equilibration runs. The common criterion of the total energy fluctuation was used to handle the energy conservation, $\Delta E(t) = [E(0) - E(t)]/E(0)$, where $E(t)$ is the total energy at time t and $E(0)$ is the initial energy.[66] Further computational details are described in refs 46 and 67. The fact that the density presents a similar decay with the water increment compared with experimental data shows that the MD simulations present reliable results regarding the liquids local structure.

4. RESULTS AND DISCUSSION

Table 1 shows the mixtures used in this study and the different ways to express the water concentration in ILs. The water

dx.doi.org/10.1021/jp312839z | J. Phys. Chem. B 2013, 117, 8782−8792

Table 1. Relationship between the Different Ways of Expressing the Amount of Water in ILs

mixture	[H_2O]		
	ppm	mol L^{-1}	x
$[BMMI][Tf_2N][H_2O]_{0.001}$	55.80	0.0040	0.0010
$[BMMI][Tf_2N]][H_2O]_{0.05}$	1990	0.15	0.023
$[BMMI][Tf_2N][H_2O]_{0.13}$	5225	0.40	0.060
$[BMMI][Tf2N][H_2O]_{0.23}$	9335	0.70	0.10
$[Li]_{0.33}[BMMI]_{0.67}[Tf_2N][H_2O]_{0.003}$	120	0.010	0.0010
$[Li]_{0.33}[BMMI]_{0.67}[Tf_2N][H_2O]_{0.08}$	3773	0.30	0.040
$[Li]_{0.33}[BMMI]_{0.67}[Tf_2N][H_2O]_{0.58}$	23273	2.2	0.22
$[Li]_{0.33}[BMMI]_{0.67}[Tf_2N][H_2O]_{1.3}$	57280	4.5	0.39

concentration reached in the Li^+ mixture is more than 6 times greater than that in the neat IL. This study will discuss the consequences on the physicochemical properties of a hydrophobic IL due to its increased capability of water absorption provoked by Li^+ addition. Table 2 shows the effect of water on

Table 2. Variation of the Electrochemical Window with the Addition of Water to the Neat IL and the Li^+ Mixture

neat IL−[H_2O]/mol L^{-1}	electrochemical window/V
0.004	3.3
0.25	2.0
0.70	1.6
Li^+ mixture−[H_2O]/mol L^{-1}	electrochemical window/V
0.01	4.0
0.25	3.1
0.4	2.4
6.5	1.6

the electrochemical window. First, it is important to notice that the Li^+ addition stabilizes the IL and provokes a wider electrochemical window due to the different structures of both systems,[44,68] even when the Li^+ mixture presents more water than the neat IL. The electrochemical window decreases with the amount of water in both cases, as expected and reported.[59] Both systems reach the same electrochemical window (1.6 V) when the neat IL contains 0.7 mol L^{-1} of water and the Li^+ mixture contains 6.5 mol L^{-1} of water.

Figure 1a presents density measurements. As already reported,[46] the addition of Li^+ salt increases the density in comparison with the neat IL due to the formation of stiffer aggregates, which decreases the volume of the system. The water increment decreases the density of both systems, $[BMMI][Tf_2N]$ and $[Li][BMMI][Tf_2N]$ because water presents a lower density than the neat IL and the Li^+ mixture. At 25 °C, there is a 0.5% density decrease between the driest and the wettest samples for the neat IL. For the Li^+ mixture, at the same temperature, there is a significant decay for higher water concentrations, and this value is 6.7% between the driest and wettest samples. The density values for the Li^+ mixture with water addition are greater than the density values for the neat IL and turn out to be equal only when 9.9 mol L^{-1} of water is added, showing clearly that even for a high amount of water in the Li^+ mixture, the formation of aggregates between Li^+ and Tf_2N^- ions in the Li^+ mixture is not completely broken by the action of water.

Figure 1b shows the density and the theoretical density variation as a function of the water content at 298 K. The

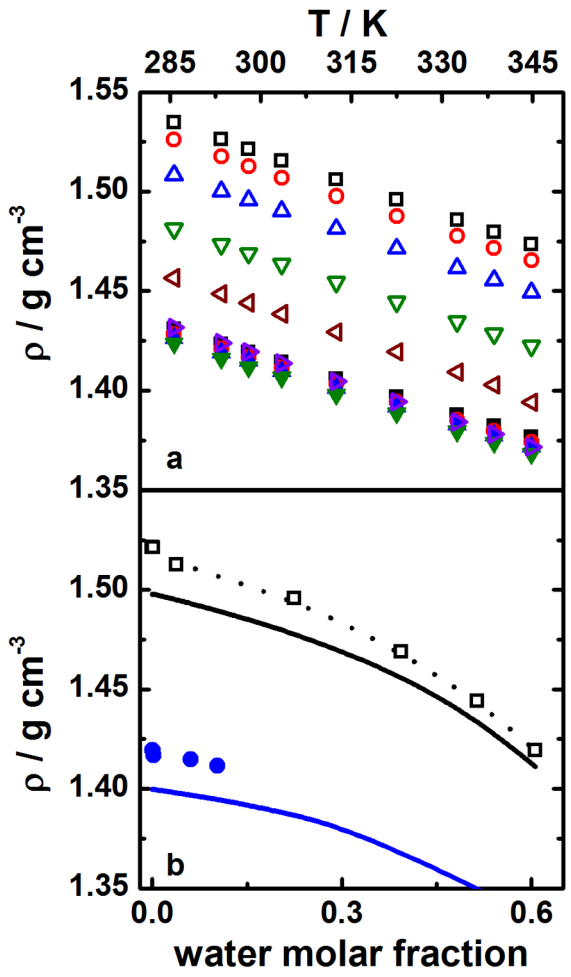

Figure 1. (a) Density at different concentrations of water as a function of temperature for neat IL (black ■ 0.004, red ● 0.15, blue ▲ 0.40, green ▼ 0.70 mol L^{-1} of water) and the Li^+ mixture (black □ 0.01, red ○ 0.30, blue △ 2.2, green ▽ 4.7, brown ◁ 7.2, purple ▷ 9.9 mol L^{-1} of water). (b) Density of the neat IL (blue ●) and of the Li^+ mixture (black □) as a function of the amount of water at 298 K. Full lines represents density values calculated from eq 2.

theoretical density was calculated by considering the volume of each ion, as proposed by Ye and Shreeve.[69]

$$\rho = \frac{W}{0.6022V} \quad (2)$$

where W is the molar mass and V is the proposed volume for each species present in the mixture. Assuming that the volume of $BMMI^+$ is 266 Å^3, Tf_2N^- is 248 Å^3, Li^+ is 1.99 Å^3,[46,69] and H_2O is 29.7 Å^3 (straight consideration from bulk water) and that the molecular formulas are $[BMMI][Tf_2N]\cdot(H_2O)_y$ and $[Li]_{0.33}[BMMI]_{0.67}[Tf_2N]\cdot(H_2O)_x$, it was possible to observe that the predicted density (lines in Figure 1b) always presented a lower value than the experimental density (dots in Figure 1b). Because the density calculation considers the theoretical volume of each species, it does not consider the interaction among ions. The interactions among the ions are strong, resulting in a lower real volume than the predicted volume. As discussed above, water interacts with the neat IL and the Li^+ mixture, resulting in a different $\rho(x_{water})$ profile. In the case of the neat IL, it is not possible to reach higher values of mole fraction because $[BMMI][Tf_2N]$ is a hydrophobic IL. For both systems, the difference between the predicted density and the

dx.doi.org/10.1021/jp312839z | J. Phys. Chem. B 2013, 117, 8782−8792

experimental density is lower with increasing water, suggesting that water decreases the interaction among ions. The densities reached in the pre-equilibrium MD simulations present a similar behavior and $\rho(x_{water})$ profile to the experimental densities because the interactions among ions are taken in account in this case, despite the temperature simulated; the values can be seen in Table 1S (Supporting Information). In this figure, it is possible to see how the presence of Li^+ can increase the IL capability to absorb water; therefore, the water addition to the Li^+ mixture and to the neat IL is a dissolution, where the water molecules play an important role in the transport properties, as discussed below.

Figure 2a shows the Arrhenius plot of the viscosity for each water concentration for both the neat IL and the Li^+ mixture.

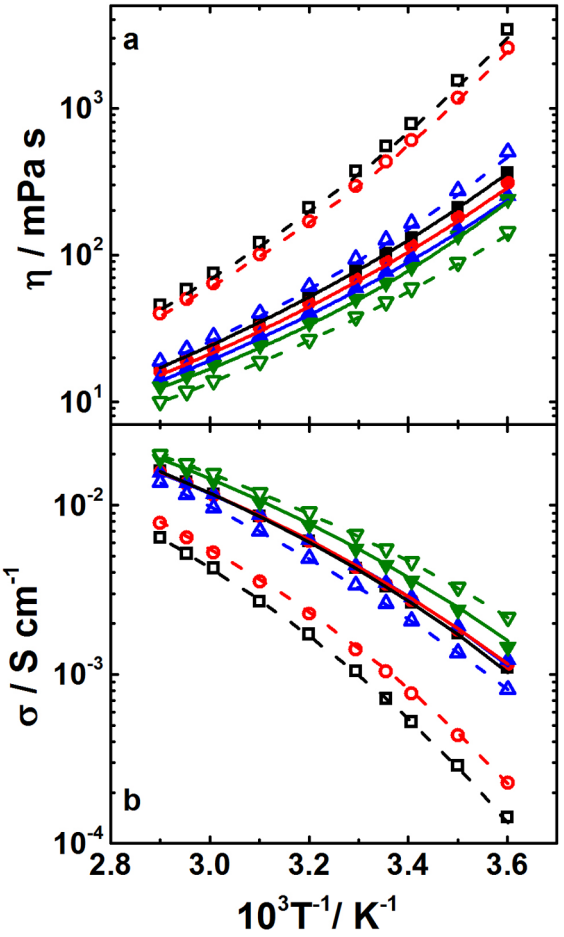

Figure 2. Arrhenius plot of the viscosity (a) and the ionic conductivity (b) for neat IL (black ■ 0.004, red ● 0.15, blue ▲ 0.40, green ▼ 0.70 mol L^{-1} of water) and for the Li^+ mixture (black □ 0.01, red ○ 0.30, blue △ 2.2, green ▽ 4.7 mol L^{-1} of water). Full lines (neat IL) and dashed lines (Li^+ mixture) are the best fits of the VTF, respectively.

The viscosity values present a diminution with the temperature for all systems. The viscosity also decreases with increasing water. This finding suggests two considerations: first, water is a less viscous solvent than the mixtures; thus, it is expected that the addition of water should decrease the viscosity. Second, as suggested by the density measurements, water molecules decrease the interactions among ions, and these lower interactions result in less stiff ion aggregates than those in a dry system, resulting in a less viscous mixture. When the Li^+ mixture contains 2.2 mol L^{-1} of water, the mixture viscosity is 20% greater than that of the dry neat IL, and when the Li^+ mixture contains 4.7 mol L^{-1} of water, its viscosity is lower than that of the neat IL.

Lines in Figure 2a represent the best fitting by the Vogel–Tammann–Fulcher (VTF) equation[70] to the viscosity

$$\eta = A \exp\left(\frac{B}{T - T_0}\right) \tag{3}$$

where A, B, and T_0 are adjustable parameters. The Vogel temperature T_0 is the temperature at which the viscosity tends to infinity.[70] T_0 does not change for the neat IL and the water increment, which remains at ∼172 K for all water concentrations studied, while for the Li^+ mixture, T_0 decreases from 178 to 168 K for the water concentrations studied, showing that the maximum viscosity is reached at a lower temperature when water is added to the Li^+ mixture. The relationship B/T_0 is related to the fragility of the liquid, which indicates how the transport properties depend on temperature; the transport coefficients of strong liquids suffer a less drastic change with temperature, whereas fragile liquids show a large modification in these properties at low temperatures.[70] The strong/fragile classification is used near the glass transition temperature, but we are considering the fragility of these systems only in the temperature range studied in this paper. Thus, the modification of the $\eta(T)$ curve at lower temperatures should be further considered.[71] The water addition in the neat IL does not have any effect on the liquid fragility, remaining at $B/T_0 \approx 4.5$ for all water concentrations; in contrast, the Li^+ mixture presents a decay of the fragility with water addition, from $B/T_0 \approx 6.0$ in the dry mixture to $B/T_0 \approx 4.5$ in wet mixtures (plot not shown). The transport properties should vary more in the wet Li^+ mixture than those in the dry one when the temperature is changed. Once again, the variation in the Li^+ mixture fragility suggests that water has a more important role in the new structure of the liquid than that in the neat IL, turning it into a less stiff system compared to the dry mixture.

Figure 2b shows the Arrhenius plot of the ionic conductivity for each water concentration for both the neat IL and the Li^+ mixture. The ionic conductivity increases with the addition of water as expected because the viscosity decreases with the water amount and the ionic conductivity is proportional to the viscosity. It is important to notice that, as with the viscosity, the addition of 2.2 mol L^{-1} of water causes the ionic conductivity of the Li^+ mixture to decrease to values 19% smaller than the dry neat IL value. This result shows the good agreement between the viscosity and ionic conductivity experiments because the viscosity of this Li^+ mixture is 20% greater than that of the dry neat IL. By increasing the temperature, the difference among the conductivities of different mixtures is decreased, as discussed below.

Figure 3 shows the Walden plot for the Li^+ mixture (Figure 3a) and the neat IL (Figure 3b), which is an effective way to analyze the relationship between the molar ionic conductivity (Λ/S cm^2 mol^{-1}), which was calculated by considering all ions present in the mixture, and the fluidity (η^{-1}/mPa^{-1} s^{-1}). According to the Walden rule, the product of the molar ionic conductivity and the viscosity must be constant for aqueous strong electrolytes,[72] and this rule is followed at lower concentrations of water for both systems, where this relationship is linear. In systems with higher water concentrations, the linearity is observed in a range of low fluidity (low

dx.doi.org/10.1021/jp312839z | J. Phys. Chem. B 2013, 117, 8782–8792

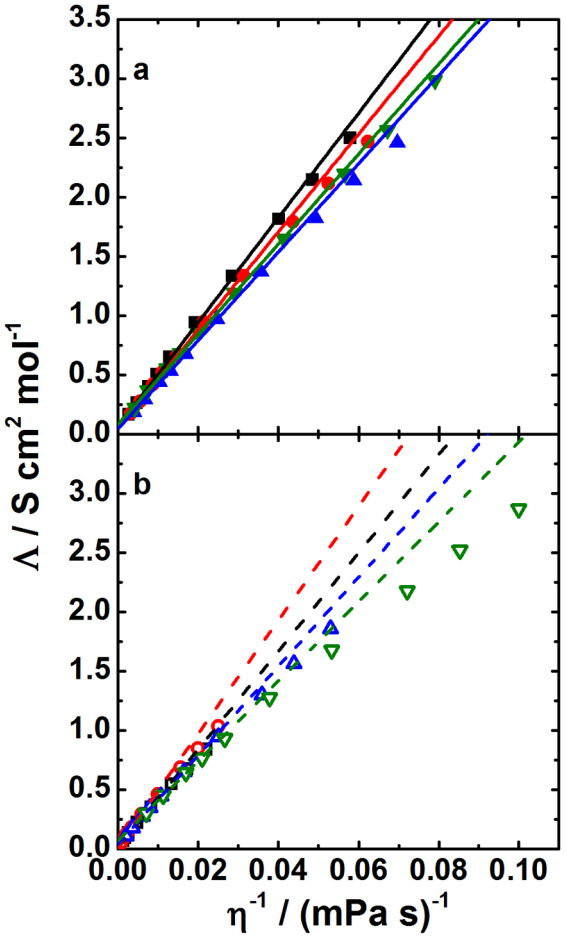

Figure 3. Relationship between the molar ionic conductivity and the fluidity for (a) neat IL (black ■ 0.004, red ● 0.15, blue ▲ 0.40, green ▼ 0.70 mol L^{-1} of water) and for (b) the Li^+ mixture (black □ 0.01, red ○ 0.30, blue △ 2.2, green ▽ 4.7 mol L^{-1} of water). Lines (a) and broken lines (b) represent the linearity in low fluidity.

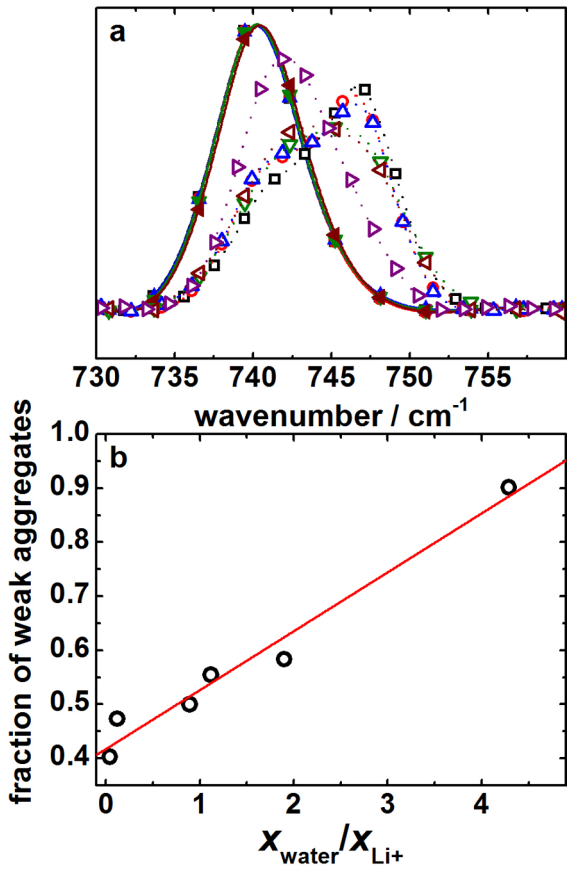

Figure 4. (a) Raman spectra of neat IL (–■– 0.004, red –●– 0.02, blue –▲– 0.03, green –▼– 0.04, brown –◀– 0.3 mol L^{-1} of water) and Li^+ mixture (--□-- 0.05, red --○-- 0.30, blue --△-- 0.40, green --▽-- 1.4, brown --◁-- 2.3, purple -- ▷-- 5.0 mol L^{-1} of water) in the region of 730–760 cm^{-1} normalized by the total area. (b) Fraction of weak aggregates as a function of the ratio between the water molar fraction and the Li^+ molar fraction. The red full line is a visual guide.

temperature), and the linearity is lost at higher fluidity. Thus, the molar ionic conductivity is lower than expected at this point; however, the fluidity is increasing, and the mass and charge transport should be facilitated. These results suggested a modification in the physicochemical nature of the Li^+ and Tf_2N^- ion aggregates, mainly in the Li^+ mixture.

An effective way to analyze a change in the Tf_2N^- anion environment is by Raman spectroscopy because the Raman spectrum of the Tf_2N^--based IL has been studied extensively.[46,48] Figure 4a presents the Raman spectra in the 730–760 cm^{-1} range, in which an intense band is observed at 740 cm^{-1} related to the expansion and contraction of the whole Tf_2N^- anion.[48] With Li^+ salt addition, the band decreases, and a new band is formed at 747 cm^{-1}; the intensity of both bands depends on the Li^+ concentration, and the ratio between the integration of the new band at 747 cm^{-1} and the whole integration between 730 and 760 cm^{-1} ($A_{747}/A_{740} + A_{747}$) is proportional to the amount of Li^+ added. The splitting of the band occurs due to the formation of two different kinds of aggregates, the weak aggregate that is related to the anion in the neat IL and the strong aggregate that is related to the anion in the coordination sphere of Li^+, as previously discussed by Lassègues et al.,[48] Umebayashi et al.,[47,49,73,74] and Monteiro et al.[46] While the addition of water to the neat IL has no effect on this band, the same is not observed for the Li^+ mixture. The addition of water to the Li^+ mixture is similar to the addition of Li^+ salt to an IL, that is, there is a change in the relative intensities of both bands. However, in this case, there is a decrease of the intensity of the band at 747 cm^{-1} and an increase of the intensity of the band at 742 cm^{-1}, indicating an increase in the amount of weak aggregates. However, the band related to the weak aggregates is now shifted to 742 cm^{-1} (for neat IL, the band is located at 740 cm^{-1}), indicating a different kind of aggregate when water is present. Another important observation that indicates the formation of different aggregates is the fact that the ionic conductivity is still smaller than that of the neat IL even with 2.2 mol L^{-1} of water added to the Li^+ mixture, as shown above.

By considering the similarity of the band shapes related to the strong and weak aggregates and assuming that the scattering cross section of both species is similar, it is possible to estimate the amount of both species as a function of the water/Li^+ molar fraction ratio by fitting the two components with Gaussian profiles. Figure 4b shows that the fraction of weak aggregates increases with the water/Li^+ molar fraction ratio, starting at ~0.4 in the driest systems and reaching ~0.9 in the wettest systems. Water molecules replace Tf_2N^- anions in Li^+ coordination, reducing the population of strong aggregates. This statement means that the presence of water reduces the

dx.doi.org/10.1021/jp312839z | J. Phys. Chem. B 2013, 117, 8782–8792

Li^+ and Tf_2N^- interactions, making strong aggregates look like weak aggregates. Note that the proportions of the Li^+/anion, Li^+/cation, and cation/anion remained fixed.

Figure 5 shows Raman spectra obtained at 293 and 345 K for neat IL and the Li^+ mixture for dry and wet systems to evaluate

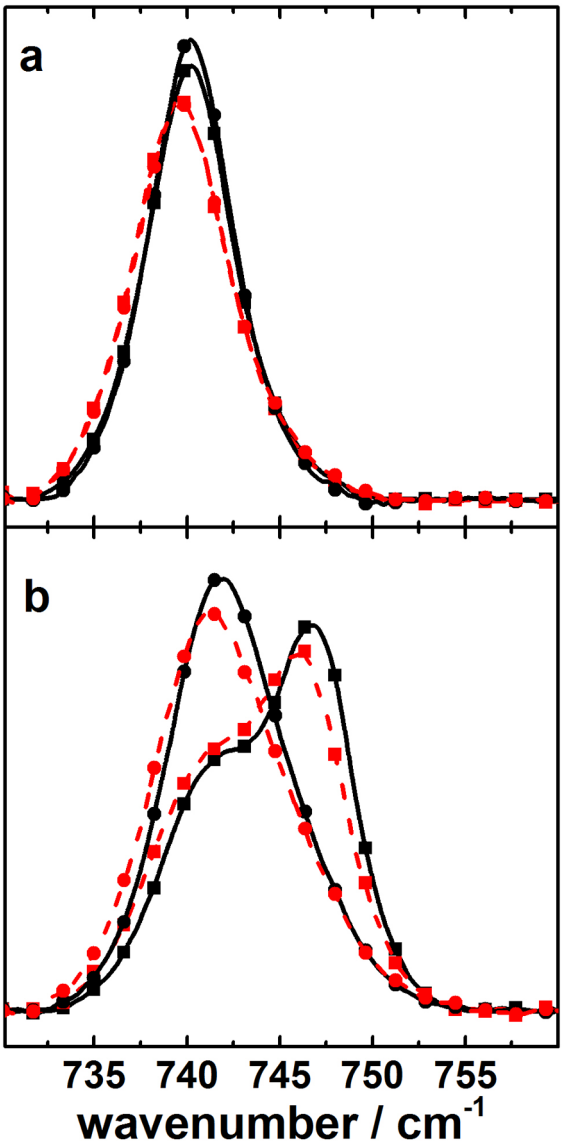

Figure 5. Raman spectra of (a) the neat IL (■ 0.004 e, ● 0.70 mol L^{-1} of water) and (b) the Li^+ mixture (■ 0.01, ● 6.25 mol L^{-1} of water) at 298 K (black symbols and full line) and 345 K (red symbols and dashed line) in the region of 730–760 cm^{-1} normalized by the total area.

whether there are different aggregates at higher temperatures, which could explain the lower increase of the molar ionic conductivity with the fluidity than expected (see Figure 3). The temperature has no effect on the population of the aggregates because the spectra are almost the same, so that the difference between the fractions of weak aggregates is insignificant. It is worth noting that the band was fit even in neat IL by considering weak and strong aggregates for a comparison between both systems. There is no evidence of new aggregate formation at different temperatures, and thus, the lower increase of ionic conductivity than expected is not related to the formation of new aggregates. Because the ionic conductivity is related to the viscosity and the effective radius, $D \propto (\eta \cdot r)^{-1}$, where D, η, and r are, respectively, the diffusion, the viscosity, and the effective radius, and viscosity is the inverse of the fluidity, the only explanation for the lower increase of ionic conductivity than expected would be the change in the effective radius. The ionic aggregate (charge carrier) presents a greater size at higher temperature, maintaining the population of the anions Tf_2N^- in the clusters, as suggested by the Raman spectra. The higher the size, the smaller the diffusion, resulting in a lower ionic conductivity.

The liquid short-range structure was evaluated by MD simulation. The local equilibrium structure was evaluated by the pair radial distribution function (rdf) between the center of mass, $g_{\alpha\beta}(r)$. Figure 6 shows the $g_{\alpha\beta}(r)$ for (a) [BMMI]–[BMMI], (b) [Tf_2N]–[Tf_2N], and (c) [BMMI]–[Tf_2N] for the neat IL with three concentrations of water, with no water[46] and water molar fractions of 0.07 and 0.10.

The first observations are the out-of-phase oscillations between [BMMI]–[BMMI] (Figure 6a), [Tf_2N]–[Tf_2N] (Figure 6b), and [BMMI]–[Tf_2N] (Figure 6c) rdfs due to

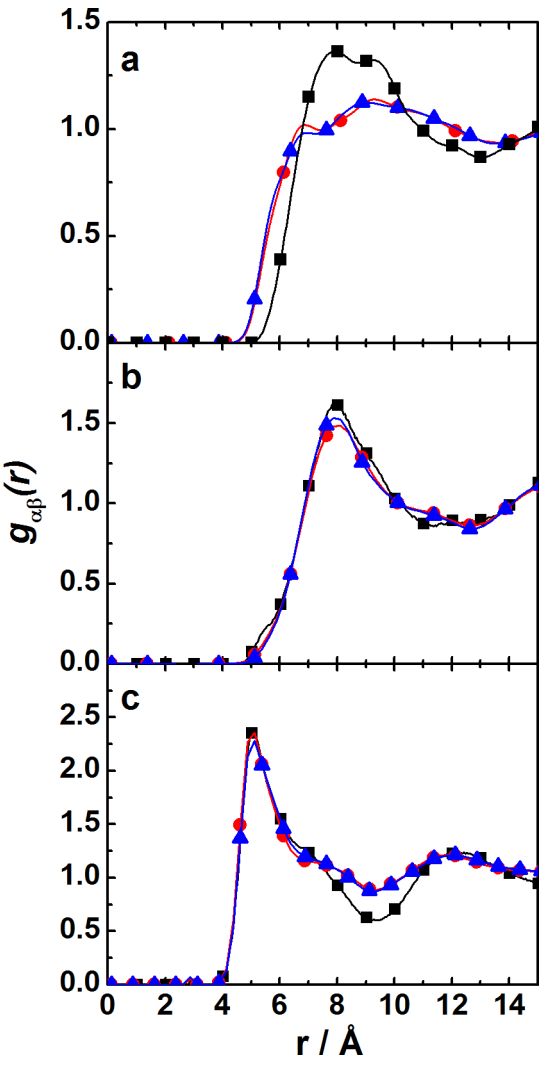

Figure 6. Partial radial distribution functions for the center of mass of (a) [BMMI], (b) [Tf_2N], and (c) the cross for the [BMMI]–[Tf_2N] term calculated by MD simulations of the neat IL by varying the water concentration for water molar fractions of (■) 0,[46] (red ●) 0.07, and (blue ▲) 0.10.

dx.doi.org/10.1021/jp312839z | J. Phys. Chem. B 2013, 117, 8782–8792

the charge ordering in the IL structure. Even when water was added to the box simulation, these out-of-phase oscillations were kept, indicating that water molecules do not change the charge ordering in the structure. The main effect of water addition is observed in the [BMMI]−[BMMI] rdf (Figure 6a), in which there is a significant decrease in the intensity of the two first peaks at ∼6.0 and 8.5 Å. The first peak seems to be a shoulder of the coordination sphere; in addition, there is a small shift in the first peak to lower r and in the second peak to larger r, showing a looser coordination in the wet systems. The first peak presents a decrease in the number of neighbors (4.3, 2.0, and 1.8) as the water concentration increases, but it has better shape definition when water is added. The second peak presents an increase in the number of neighbors upon water addition (12.4, 16.5, 18.8); this will be discussed again later; note that the numbers of neighbors were calculated by integrating the $g_{\alpha\beta}(r)$ up to the minimum after the cited peak (e.g., 8.7 and 13.0 Å for the dry neat IL). The rdfs between the anions (Figure 6b) do not show a significant change but only a slight decrease in the intensity while maintaining the same profile; this will be also discussed later. This finding is in line with the conclusions drawn from the Raman spectra (see Figure 4) that the addition of water in the neat IL does not have an impact in the anion neighborhood, regarding the ions. The rdfs between the cation and anion (Figure 6c) present a similar profile for the three water concentrations; however, the dry system presents a deeper minimum around 10 Å than the wet systems, and this is related to the organization of the coordination shells. The first and second peaks of the neighbors are more defined in the dry case. Water addition breaks the local structure of cation−anion aggregates, forming a less organized ionic pair than that in the dry case. The presence of water between the cation and anion shells leads to a looser organization among ions, impacting the cation−cation and anion−anion rdfs. In the cation−cation rdfs, the diminution in the first neighbors leads to an increase of the importance of the second neighbors, and this coordination sphere is spread in larger r than that in the dry system. This explains the fact that the second neighbor's number was increased by ∼4 cations upon water addition from dry to a 0.07 water molar fraction and by ∼2.5 cations upon water addition from a 0.07 to 0.10 water molar fraction. Therefore, the second neighbor's number increases by 6.5 cations and the first neighbor's number diminishes by 2.5, leading to a net coordination sphere (the sum of the shoulder and peak) of 4 cations from dry to a 0.10 water molar fraction due this looser coordination. In the case of anion−anion rdfs, there is a slight diminution in the anions population due to water presence, but the charge ordering is kept upon water addition, as already discussed.

Figure 7 presents the rdfs of the center of mass of [BMMI]−[BMMI], [Tf_2N]−[Tf_2N], [BMMI]−[Tf_2N], and [Tf_2N]−[Li] for the Li^+ mixture at three water concentrations (dry and water molar fractions of 0.14 and 0.40). The [BMMI]−[BMMI] rdf (Figure 7a) shows a small change when water is added to the Li^+ mixtures. This first peak (coordination sphere shoulder) observed in the neat IL case (Figure 6a) is not present in Li^+ mixtures (Figure 7a) due to the new aggregates formed when the metallic cation is present. As stiffer aggregates are formed, the compaction of the liquid increases, so that the coordination sphere shoulder loses importance. In the neat IL case, the water addition results in a well-define first peak, and in the Li^+ mixture case, a shoulder appears at smaller r with the water increment, leading to a similar shape as that in the case of neat

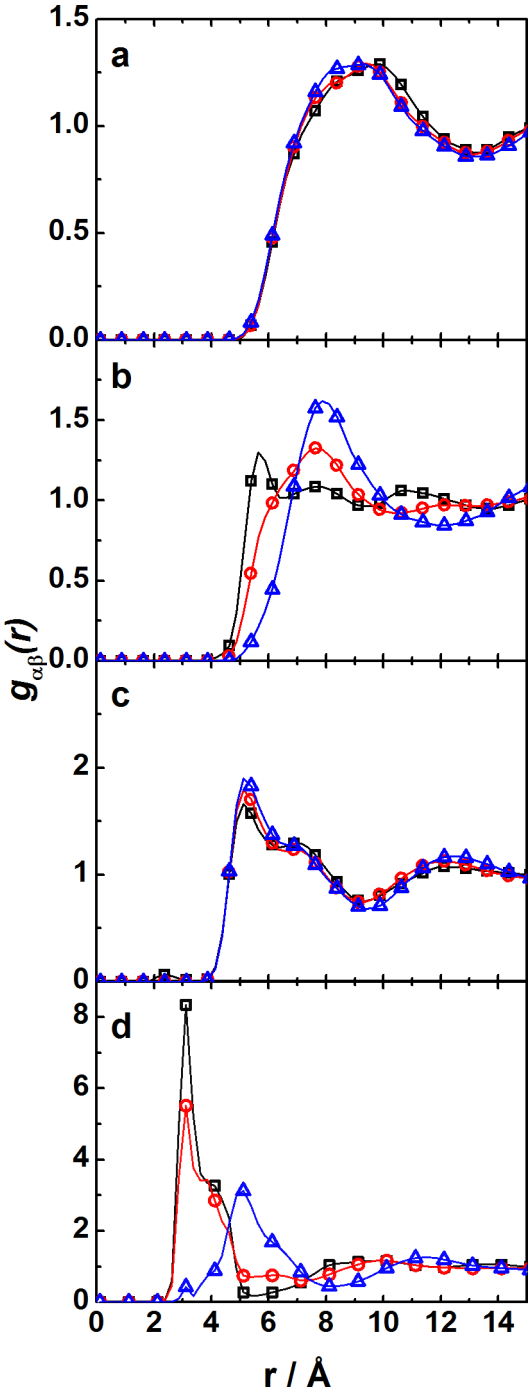

Figure 7. Partial radial distribution functions for the center of mass of (a) [BMMI], (b) [Tf_2N], (c) the cross term [BMMI]−[Tf_2N], and (d) Li^+−[Tf_2N] as calculated by MD simulations of the Li^+ mixture with varying water concentrations of water molar fractions of (black □) 0, (red ○) 0.14, and (blue △) 0.40.

IL. The [Tf_2N]−[Tf_2N] rdf shows a greater modification when Li^+ is present due to the formation of stiffer aggregates between the metallic cation and the anion, as already reported by Monteiro et al.[46] (see Figures 6b and 7b). These aggregates are mainly affected by the addition of water (Figure 7b), and the profile of the $g_{[Tf2N]\text{-}[Tf2N]}(r)$ reaches exactly the same profile as that of the neat IL when a 0.40 molar fraction of water is added. The intermediary concentration of water presents a transition profile between the other two structures, which is also observed

dx.doi.org/10.1021/jp312839z | J. Phys. Chem. B 2013, 117, 8782−8792

in the Raman spectra in Figure 4. The cross term for the [BMMI]−[Tf_2N] rdf (Figure 7c) presents a similar profile as the [BMMI]−[Tf_2N] rdf in neat IL (Figure 6c). When more water is added to the Li^+ mixture, the first peak increases, reaching ∼1.9 versus ∼2.3 for the neat IL. This change is expected because Li^+ cations are solvated by water molecules and the structure of the mixture becomes similar to that of the neat IL. The rdf of the cross term for [Tf_2N]−[Li] (Figure 7d) presents a drastic reduction in the intensity from the dry system to a water molar fraction of 0.40, and the first peak is dislocated to larger *r*. Moreover, the number of neighbors presents a small decrease from 1.2 to 0.9 upon the first water addition, while the further increase of water produces an increase of the number of neighbors up to 7.5, as can be calculated from the integration of the spread peak caused by the loss of compaction of the coordination sphere. These 7.5 anions are spread out around the hydrated Li^+ as a second sphere coordination.

Figure 8a shows the rdfs for [BMMI]−H_2O for neat IL and Li^+ mixtures, and it can be seen that the profile does not change when the water concentration increases, but the presence of Li^+ produces an important impact on this rdf function, shifting the first peak to higher *r* values. This occurs because water molecules interact preferentially with Li^+, and in this way, the distance between [BMMI] and water increases. Figure 1S (Supporting Information) shows this effect, the profile of the [BMMI]−Li^+ rdf being very similar to that of the [BMMI]−H_2O in both water concentrations.

Figure 8b shows the [Tf_2N]−H_2O rdfs for neat IL and Li^+ mixtures. The neat IL rdfs present the same profile for both water concentrations, showing two well-defined peaks in the first solvation shell in the same region of the [BMMI]−H_2O rdf peak. This suggests that water molecules do not interact preferentially with any ion in the neat IL, and the number of neighbors between the ions and water confirms this observation. They were calculated to be almost the same (0.5 for a 0.07 water molar fraction and 0.7 for the 0.10 water molar fraction), so that in the neat IL, water molecules interact preferentially among themselves. Figure 2S (Supporting Information) shows the H_2O−H_2O rdfs where the first peak appears at smaller *r* than that for [BMMI]−H_2O and [Tf_2N]−H_2O rdfs, showing that water forms aggregates. Li^+ mixtures present different profiles for [Tf_2N]−H_2O rdfs when the water concentration increases; for the 0.14 water molar fraction, a single peak is observed, while the same neat IL profile is obtained for the 0.40 water molar fraction (two peaks in the first solvation shell). This occurs because at lower water concentrations, the anion still plays an important role in Li^+ coordination, consequently getting closer to water molecules. On the other hand, at higher water concentrations, the anion loses importance in Li^+ coordination because water will coordinate the metallic cation. In addition, it is important to point out that the high intensity obtained in the H_2O−H_2O rdfs (Figure 2S, Supporting Information) is related to the large density of the systems and the water aggregates inside of a very packed ionic system.

Figure 8c presents Li^+−H_2O rdfs for both water concentrations, where there is a very well-defined first peak at 1.835 and 1.875 Å with a number of neighbors of 1.0 and 3.8 for lower and higher water concentrations, respectively. This occurs because as the number of water molecules decreases, the interaction between Li^+ and water is strengthened. After ∼3.0 Å, secondary peaks in both cases can be observed, and they are more intense for lower water concentrations due to the

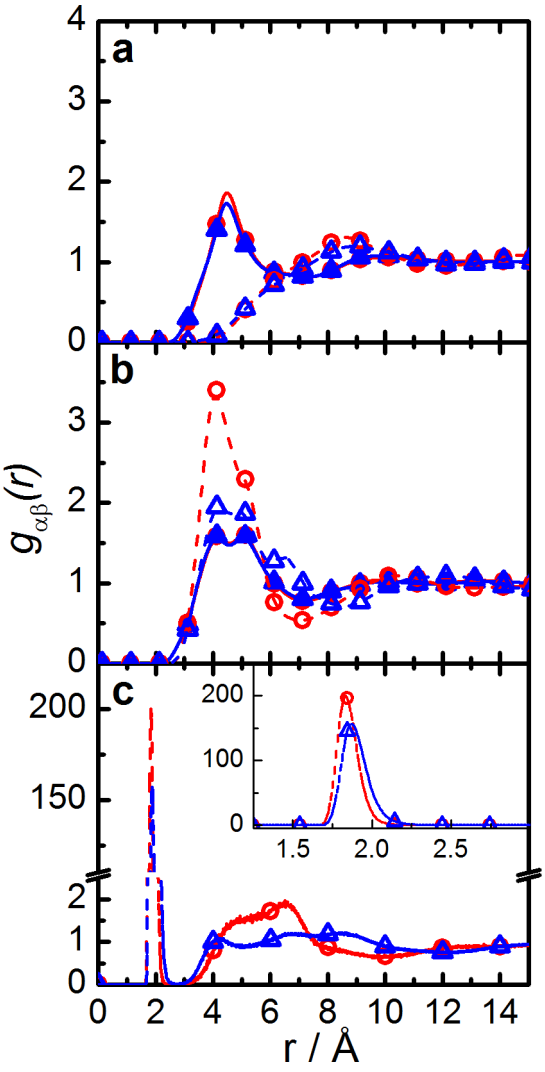

Figure 8. Partial radial distribution functions for the cross term between the center of the mass of ions and H_2O for (a) [BMMI], (b) [Tf_2N], and (c) Li^+ for the neat IL (full line) with water molar fractions of (red ●) 0.07 and (blue ▲) 0.10 and the Li^+ mixture (dashed line) with water molar fractions of (red ○) 0.14 and (blue △) 0.40 as calculated by MD simulations. Inset: region of the first peak in the Li^+−H_2O rdfs.

change in density of each system. At lower water concentration, aggregates still present some rigidity due to Li^+−[Tf_2N] interaction, and the density of the systems is higher; therefore, the water−metallic cation−anion aggregates are tight, resulting in a second solvation shell. At high water concentration, the density is lower due to the formation of less tight aggregates and to the loss of the second solvation shell.

Thus, the disruption of aggregates suggested by experiments was corroborated by the MD simulation, which showed that water plays an important role in the new aggregates in the Li^+ mixture.

Figure 9 shows snapshots of the wettest systems for the neat IL (a) and the Li^+ mixture (b); for a better understanding, the molecules representing the IL are not shown. In the neat IL, the water molecules are sparse in the simulated box, but few aggregates of water are formed, indicating the formation of water clusters in the IL, as already shown by Figure 8 and as shown by Jiang et al.[26] In the Li^+ mixture, the proportion of H_2O/Li^+ is 4, which is the exact proportion observed in the

dx.doi.org/10.1021/jp312839z | J. Phys. Chem. B 2013, 117, 8782−8792

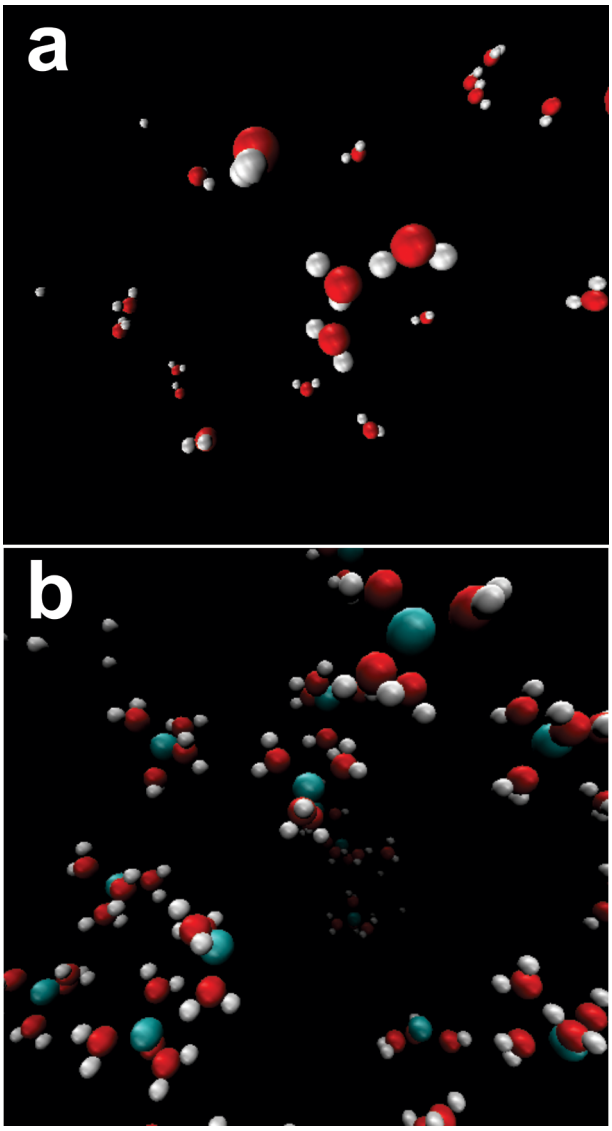

Figure 9. Arbitrary snapshots taken from the MD simulations of the wettest system simulated for the neat IL (a) and the Li^+ mixture (b), where the white, red, and green atoms are hydrogen, oxygen, and lithium, respectively. Note: the IL atoms are hidden for better visualization.

lithium coordination; the water molecules replace the Tf_2N^- anion in the metallic cation coordination. Therefore, Raman spectroscopy and MD simulations corroborate the breakage of aggregates caused by the addition of water and suggested by the analysis of the transport properties.

5. CONCLUSIONS

The amount of water that the hydrophobic IL [BMMI][Tf_2N] and its Li^+ mixture absorb in an open environment is sufficient to modify the transport properties and the local structure of the systems. The presence of lithium salt increases the capacity of water absorption due the interaction between Li^+ and the water molecules. Water absorption decreases the viscosity and increases the ionic conductivity, but the molar ionic conductivity is lower than expected in the high fluidity regime. This finding shows a break in the Stoke's law and, in our view, suggests that the size of ionic aggregates increases at high temperature and decreases the mobility of the charge carrier without modifying the Tf_2N^- anion population in the ionic aggregates. In neat IL, water forms small clusters, decreasing the organization between the cation and anion, but it is not enough to break the charge ordering of the ions and in Li^+ mixtures; the addition of water leads the strong aggregates to look like weak ones. Water molecules interact mainly with the lithium cation to change the neighbors of the Tf_2N^- anion, as was shown by Raman spectroscopy and MD simulations.

■ ASSOCIATED CONTENT

Ⓢ Supporting Information

Table 1S presents additional information of the simulated systems. Figure 1S presents [BMMI]−Li^+ and [BMMI]−H_2O rdfs, and Figure 2S presents H_2O−H_2O rdfs. Data regarding the density, viscosity, ionic conductivity, and molar ionic conductivity for all of the mixtures studied in this work are presented in Tables 2S−11S. This material is available free of charge via the Internet at http://pubs.acs.org.

■ AUTHOR INFORMATION

Corresponding Author

*E-mail: rtorresi@iq.usp.br. Phone: +55-11-30919194. Fax: +55-11-38155640.

Present Address

§B.G.N.: School of Chemical Sciences, University of Illinois at Urbana−Champaign, Urbana, Illinois 61801, United States.

Notes

The authors declare no competing financial interest.

■ ACKNOWLEDGMENTS

The authors acknowledge CNPq and FAPESP (09/53199-3) for financial support. V.L.M. thanks FAPESP (09/09209-4) for the fellowship.

■ REFERENCES

(1) Parvulescu, V. I.; Hardacre, C. Catalysis in Ionic Liquids. *Chem. Rev.* **2007**, *107*, 2615−2665.
(2) Sheldon, R. Catalytic Reactions in Ionic Liquids. *Chem. Commun.* **2001**, 2399−2407.
(3) Gordon, C. M. New Developments in Catalysis Using Ionic Liquids. *Appl. Catal., A* **2001**, *222*, 101−117.
(4) Welton, T. Room-Temperature Ionic Liquids. Solvents for Synthesis and Catalysis. *Chem. Rev.* **1999**, *99*, 2071−2083.
(5) Miao, W.; Chan, T. H. Ionic-Liquid-Supported Synthesis: A Novel Liquid-Phase Strategy for Organic Synthesis. *Acc. Chem. Res.* **2006**, *39*, 897−908.
(6) Zhao, H.; Malhotra, S. V Applications of Ionic Liquids in Organic Synthesis. *Aldrichimica Acta* **2002**, *35*, 75−83.
(7) Prowald, A.; Zein El Abedin, S.; Borisenko, N.; Endres, F. Electrodeposition of Lithium/Polystyrene Composite Electrodes from an Ionic Liquid: First Attempts. *Z. Phys. Chem.* **2012**, *226*, 121−128.
(8) Cheek, G. T.; O'Grady, W. E.; El Abedin, S. Z.; Moustafa, E. M.; Endres, F. Studies on the Electrodeposition of Magnesium in Ionic Liquids. *J. Electrochem. Soc.* **2008**, *155*, D91−D95.
(9) Martindale, B. C. M.; Ward Jones, S. E.; Compton, R. G. A Comparison of the Cyclic Voltammetry of the Sn/Sn(II) Couple in the Room Temperature Ionic Liquids *N*-Butyl-*N*-methylpyrrolidinium Dicyanamide and *N*-Butyl-*N*-methylpyrrolidinium Bis-(trifluoromethylsulfonyl)imide: Solvent Induced Changes of Electrode Reaction Mechanism. *Phys. Chem. Chem. Phys.* **2010**, *12*, 1827−33.
(10) Zeinelabedin, S.; Saad, A.; Farag, H.; Borisenko, N.; Liu, Q.; Endres, F. Electrodeposition of Selenium, Indium and Copper in an Air- and Water-Stable Ionic Liquid at Variable Temperatures. *Electrochim. Acta* **2007**, *52*, 2746−2754.

(11) Kakibe, T.; Yoshimoto, N.; Egashira, M.; Morita, M. Optimization of Cation Structure of Imidazolium-Based Ionic Liquids as Ionic Solvents for Rechargeable Magnesium Batteries. *Electrochem. Commun.* **2010**, *12*, 1630−1633.
(12) Yoshimoto, N.; Matsumoto, M.; Egashia, M.; Morita, M. Mixed Electrolyte Consisting of Ethylmagnesiumbromide with Ionic Liquid for Rechargeable Magnesium Electrode. *J. Power Sources* **2010**, *195*, 2096−2098.
(13) Lewandowski, A.; Świderska-Mocek, A. Ionic liquids as Electrolytes for Li-Ion Batteries—An Overview of Electrochemical Studies. *J. Power Sources* **2009**, *194*, 601−609.
(14) Tsuda, T.; Hussey, C. L. Electrochemical Applications of Room-Temperature Ionic Liquids. *Electrochem. Soc. Interface* **2007**, 42−49.
(15) Menezes, W. G.; Reis, D. M.; Benedetti, T. M.; Oliveira, M. M.; Soares, J. F.; Torresi, R. M.; Zarbin, A. J. G. V_2O_5 Nanoparticles Obtained from a Synthetic Bariandite-Like Vanadium Oxide: Synthesis, Characterization and Electrochemical Behavior in an Ionic Liquid. *J. Colloid Interface Sci.* **2009**, *337*, 586−93.
(16) Armand, M.; Endres, F.; MacFarlane, D. R.; Ohno, H.; Scrosati, B. Ionic Liquid Materials for the Electrochemical Challenges of the Future. *Nat. Mater.* **2009**, *8*, 621−629.
(17) Monteiro, M. J.; Camilo, F. F.; Ribeiro, M. C. C.; Torresi, R. M. Ether-Bond-Containing Ionic Liquids and the Relevance of the Ether Bond Position to Transport Properties. *J. Phys. Chem. B* **2010**, *114*, 12488−12494.
(18) Bazito, F.; Kawano, Y.; Torresi, R. Synthesis and Characterization of Two Ionic Liquids with Emphasis on Their Chemical Stability Towards Metallic Lithium. *Electrochim. Acta* **2007**, *52*, 6427−6437.
(19) Endres, F. Physical Chemistry of Ionic Liquids. *Phys. Chem. Chem. Phys.* **2010**, *12*, 1649−1658.
(20) Widegren, J. A.; Laesecke, A.; Magee, J. W. The Effect of Dissolved Water on the Viscosities of Hydrophobic Room-Temperature Ionic Liquids. *Chem. Commun.* **2005**, 1610−1612.
(21) Jacquemin, J.; Husson, P. Density and Viscosity of Several Pure and Water-Saturated Ionic Liquids. *Green. Chem.* **2006**, 172−180.
(22) Seddon, K. R.; Stark, A.; Torres, M.-J. Influence of Chloride, Water, and Organic Solvents on the Physical Properties of Ionic Liquids. *Pure Appl. Chem.* **2000**, *72*, 2275−2287.
(23) Liu, W.; Zhao, T.; Zhang, Y.; Wang, H.; Yu, M. The Physical Properties of Aqueous Solutions of the Ionic Liquid [BMIM][BF4]. *J. Solution Chem.* **2006**, *35*, 1337−1346.
(24) Rodriguez, J.; Elola, M. D.; Laria, D. Ionic Liquid Aqueous Solutions under Nanoconfinement. *J. Phys. Chem. C* **2012**, *116*, 5394−5400.
(25) Sturlaugson, A. L.; Fruchey, K. S.; Fayer, M. D. Orientational Dynamics of Room Temperature Ionic Liquid/Water Mixtures: Water-Induced Structure. *J. Phys. Chem. B* **2012**, *116*, 1777−1787.
(26) Jiang, W.; Wang, Y.; Voth, G. A. Molecular Dynamics Simulation of Nanostructural Organization in Ionic Liquid/Water Mixtures. *J. Phys. Chem. B* **2007**, *111*, 4812−4818.
(27) Feng, S.; Voth, G. A. Molecular Dynamics Simulations of Imidazolium-Based Ionic Liquid/Water Mixtures: Alkyl Side Chain Length and Anion Effects. *Fluid Phase Equilib.* **2010**, *294*, 148−156.
(28) Jeon, J.; Kim, H.; Goddard, W. A.; Pascal, T. A.; Lee, G.-I.; Kang, J. K. The Role of Confined Water in Ionic Liquid Electrolytes for Dye-Sensitized Solar Cells. *J. Phys. Chem. Lett.* **2012**, *3*, 556−559.
(29) Blesic, M.; Marques, M. H.; Plechkova, N. V.; Seddon, K. R.; Rebelo, L. P. N.; Lopes, A. Self-Aggregation of Ionic Liquids: Micelle Formation in Aqueous Solution. *Green. Chem.* **2007**, *9*, 481−490.
(30) Niazi, A. A.; Rabideau, B. D.; Ismail, A. E. Effects of Water Concentration on the Structural and Diffusion Properties of Imidazolium-Based Ionic Liquid−Water Mixtures. *J. Phys. Chem. B* **2013**, *117*, 1378−1388.
(31) Yasaka, Y.; Klein, M. L.; Nakahara, M.; Matubayasi, N. Rotational Dynamics of Benzene and Water in an Ionic Liquid Explored via Molecular Dynamics Simulations and NMR T1Measurements. *J. Chem. Phys.* **2012**, *136*, 74508−74512.
(32) Kimura, H.; Yasaka, Y.; Nakahara, M.; Matubayasi, N. Nuclear Magnetic Resonance Study on Rotational Dynamics of Water and Benzene in a Series of Ionic Liquids: Anion and Cation Effects. *J. Chem. Phys.* **2012**, *137*, 194503−194510.
(33) Galinski, M.; Lewandowski, A.; Stepniak, I. Ionic Liquids as Electrolytes. *Electrochim. Acta* **2006**, *51*, 5567−5580.
(34) Hardwick, L. J.; Holzapfel, M.; Wokaun, A.; Novak, P. Raman Study of Lithium Coordination in EMI-TFSI Additive Systems as Lithium-Ion Battery Ionic Liquid Electrolytes. *J. Raman Spectrosc.* **2007**, *38*, 110−112.
(35) Holzapfel, M.; Jost, C.; Novak, P. Stable Cycling of Graphite in an Ionic Liquid Based Electrolyte. *Chem. Commun.* **2004**, 2098−2099.
(36) Holzapfel, M.; Jost, C.; Prodi-Schwab, A.; Krumeich, F.; Wursig, A.; Buqa, H.; Novak, P. Stabilisation of Lithiated Graphite in an Electrolyte Based on Ionic Liquids: An Electrochemical and Scanning Electron Microscopy Study. *Carbon* **2005**, *43*, 1488−1498.
(37) Winter, M.; Besenhard, J. O.; Spahr, M. E.; Novak, P. Insertion Electrode Materials for Rechargeable Lithium Batteries. *Adv. Mater.* **1998**, *10*, 725−763.
(38) Tarascon, J. M.; Armand, M. Issues and Challenges Facing Rechargeable Lithium Batteries. *Nature* **2001**, *414*, 359−367.
(39) Spahr, M. E.; Novák, P.; Haas, O.; Nesper, R. Electrochemical Insertion of Lithium, Sodium and Magnesium in Molybdenum (VI) Oxide. *J. Power Sources* **1995**, *54*, 346−351.
(40) Seki, S.; Kobayashi, Y.; Miyashiro, H.; Ohno, Y.; Usami, A.; Mita, Y.; Kihira, N.; Watanabe, M.; Terada, N. Lithium Secondary Batteries Using Modified-Imidazolium Room-Temperature Ionic Liquid. *J. Phys. Chem. B* **2006**, *110*, 10228−10230.
(41) Howlett, P. C.; MacFarlane, D. R.; Hollenkamp, A. F. High Lithium Metal Cycling Efficiency in a Room-Temperature Ionic Liquid. *Electrochem. Solid-State Lett.* **2004**, *7*, A97−A101.
(42) Garcia, B.; Lavallée, S.; Perron, G.; Michot, C.; Armand, M. Room Temperature Molten Salts as Lithium Battery Electrolyte. *Electrochim. Acta* **2004**, *49*, 4583−4588.
(43) Zheng, H.; Jiang, K.; Abe, T.; Ogumi, Z. Electrochemical Intercalation of Lithium into a Natural Graphite Anode in Quaternary Ammonium-Based Ionic Liquid Electrolytes. *Carbon* **2006**, *44*, 203−210.
(44) Fukuda, Y.; Tanaka, R.; Tshikawa, M. Beneficial Effects of a Li Salt on Electrode Behavior in an Ionic Liquid for Electric Double Layer Capacitors. *Electrochemistry* **2007**, *75*, 589−591.
(45) Endres, F.; Zein El Abedin, S. Air and Water Stable Ionic Liquids in Physical Chemistry. *Phys. Chem. Chem. Phys.* **2006**, *8*, 2101−2116.
(46) Monteiro, M. J.; Bazito, F. F. C.; Siqueira, L. J. A.; Ribeiro, M. C. C.; Torresi, R. M. Transport Coefficients, Raman Spectroscopy, and Computer Simulation of Lithium Salt Solutions in an Ionic Liquid. *J. Phys. Chem. B* **2008**, *112*, 2102−2109.
(47) Umebayashi, Y.; Mitsugi, T.; Fukuda, S.; Fujimori, T.; Fujii, K.; Kanzaki, R.; Takeuchi, M.; Ishiguro, S.-I. Lithium Ion Solvation in Room-Temperature Ionic Liquids Involving Bis(trifluoromethanesulfonyl)imide Anion Studied by Raman Spectroscopy and DFT Calculations. *J. Phys. Chem. B* **2007**, *111*, 13028−13032.
(48) Lassegues, J.-C.; Grondin, J.; Talaga, D. Lithium Solvation in Bis(trifluoromethanesulfonyl)imide-Based Ionic Liquids. *Phys. Chem. Chem. Phys.* **2006**, *8*, 5629−5632.
(49) Umebayashi, Y.; Harnano, H.; Seki, S.; Minofar, B.; Fujii, K.; Hayamizu, K.; Tsuzuki, S.; Kameda, Y.; Kohara, S.; Watanabe, M. Liquid Structure of and Li^+ Ion Solvation in Bis(trifluoromethanesulfonyl)amide Based Ionic Liquids Composed of 1-Ethyl-3-methylimidazolium and *N*-Methyl-*N*-propylpyrrolidinium Cations. *J. Phys. Chem. B* **2011**, *115*, 12179−12191.
(50) Nicolau, B. G.; Sturlaugson, A.; Fruchey, K.; Ribeiro, M. C. C.; Fayer, M. D. Room Temperature Ionic Liquid−Lithium Salt Mixtures: Optical Kerr Effect Dynamical Measurements. *J. Phys. Chem. B* **2010**, *114*, 8350−8356.
(51) Zhou, Q.; Boyle, P. D.; Malpezzi, L.; Mele, A.; Shin, J.-H.; Passerini, S.; Henderson, W. A. Phase Behavior of Ionic Liquid−LiX

Mixtures: Pyrrolidinium Cations and $TFSI^-$ Anions — Linking Structure to Transport Properties. *Chem. Mater.* **2011**, *23*, 4331−4337.
(52) Niu, S.; Cao, Z.; Li, S.; Yan, T. Structure and Transport Properties of the $LiPF_6$ Doped 1-Ethyl-2,3-dimethyl-imidazolium Hexafluorophosphate Ionic Liquids: A Molecular Dynamics Study. *J. Phys. Chem. B* **2009**, *114*, 877−881.
(53) Umecky, T.; Saito, Y.; Okumura, Y.; Maeda, S.; Sakai, T. Ionization Condition of Lithium Ionic Liquid Electrolytes under the Solvation Effect of Liquid and Solid Solvents. *J. Phys. Chem. B* **2008**, *112*, 3357−3364.
(54) Figueiredo, P. H.; Siqueira, L. J. A.; Ribeiro, M. C. C. The Equilibrium Structure of Lithium Salt Solutions in Ether-Functionalized Ammonium Ionic Liquids. *J. Phys. Chem. B* **2012**, *116*, 12319−12324.
(55) Widegren, J. A.; Magee, J. W. Density, Viscosity, Speed of Sound, and Electrolytic Conductivity for the Ionic Liquid 1-Hexyl-3-methylimidazolium Bis(trifluoromethylsulfonyl)imide and Its Mixtures with Water. *J. Chem. Eng. Data* **2007**, *52*, 2331−2338.
(56) Kelkar, M. S.; Maginn, E. J. Effect of Temperature and Water Content on the Shear Viscosity of the Ionic Liquid 1-Ethyl-3-methylimidazolium Bis(trifluoromethanesulfonyl)imide as Studied by Atomistic Simulations. *J. Phys. Chem. B* **2007**, *111*, 4867−7486.
(57) Römich, C.; Merkel, N. C.; Valbonesi, A.; Schaber, K.; Sauer, S.; Schubert, T. J. S. Thermodynamic Properties of Binary Mixtures of Water and Room-Temperature Ionic Liquids: Vapor Pressures, Heat Capacities, Densities, and Viscosities of Water + 1-Ethyl-3-methylimidazolium Acetate and Water + Diethylmethylammonium Methane Sulfonate. *J. Chem. Eng. Data* **2012**, *57*, 2258−2264.
(58) Widegren, J. A.; Saurer, E. M.; Marsh, K. N.; Magee, J. W. Electrolytic Conductivity of Four Imidazolium-Based Room-Temperature Ionic Liquids and the Effect of a Water Impurity. *J. Chem. Thermodyn.* **2005**, *37*, 569−575.
(59) Schroder, U.; Wadhawan, J. D.; Compton, R. G.; Marken, F.; Suarez, P. A. Z.; Consorti, C. S.; De Souza, R. F.; Dupont, J. Water-Induced Accelerated Ion Diffusion: Voltammetric Studies in 1-Methyl-3-[2,6-(S)-dimethylocten-2-yl]imidazolium Tetrafluoroborate, 1-Butyl-3-methylimidazolium Tetrafluoroborate and Hexafluorophosphate Ionic Liquids. *New J. Chem.* **2000**, *24*, 1009−1015.
(60) Morrow, T. I.; Maginn, E. J. Molecular Dynamics Study of the Ionic Liquid 1-*n*-Butyl-3-methylimidazolium Hexafluorophosphate. *J. Phys. Chem. B* **2002**, *106*, 12807−12813.
(61) Canongia Lopes, J. N.; Pádua, A. A. H. Molecular Force Field for Ionic Liquids Composed of Triflate or Bistriflylimide Anions. *J. Phys. Chem. B* **2004**, *108*, 16893−16898.
(62) Borodin, O.; Smith, G. D. Structure and Dynamics of *N*-Methyl-*N*-propylpyrrolidinium Bis(trifluoromethanesulfonyl)imide Ionic Liquid from Molecular Dynamics Simulations. *J. Phys. Chem. B* **2006**, *110*, 11481−11490.
(63) Wu, Y.; Tepper, H. L.; Voth, G. A. Flexible Simple Point-Charge Water Model with Improved Liquid-State Properties. *J. Chem. Phys.* **2006**, *124*, 24503−24512.
(64) Martínez, L.; Andrade, R.; Birgin, E. G.; Martínez, J. M. PACKMOL: A Package for Building Initial Configurations for Molecular Dynamics Simulations. *J. Comput. Chem.* **2009**, *30*, 2157−2164.
(65) Swope, W. C.; Andersen, H. C.; Berens, P. H.; Wilson, K. R. A computer Simulation Method for the Calculation of Equilibrium Constants for the Formation of Physical Clusters of Molecules: Application to Small Water Clusters. *J. Chem. Phys.* **1982**, *76*, 637−649.
(66) Figueirido, F.; Levy, R. M.; Zhou, R.; Berne, B. J. Large Scale Simulation of Macromolecules in Solution: Combining the Periodic Fast Multipole Method with Multiple Time Step Integrators. *J. Chem. Phys.* **1997**, *106*, 9835−9849.
(67) Urahata, S. M.; Ribeiro, M. C. C. Structure of Ionic Liquids of 1-Alkyl-3-methylimidazolium Cations: A Systematic Computer Simulation Study. *J. Chem. Phys.* **2004**, *120*, 1855−1863.
(68) Matsumoto, H.; Kageyama, H.; Miyazaki, Y. Effect of Ionic Additives on the Limiting Cathodic Potential of EMI-Based Room Temperature Ionic Liquids. *Electrochemistry* **2003**, *71*, 1058−1060.
(69) Ye, C.; Shreeve, J. M. Rapid and Accurate Estimation of Densities of Room-Temperature Ionic Liquids and Salts. *J. Phys. Chem. A* **2007**, *111*, 1456−1461.
(70) Angell, C. A. Liquid Fragility and the Glass Transition in Water and Aqueous Solutions. *Chem. Rev.* **2002**, *102*, 2627−2650.
(71) Ribeiro, M. C. C. Low-Frequency Raman Spectra and Fragility of Imidazolium Ionic Liquids. *J. Chem. Phys.* **2010**, *133*, 024503.
(72) Xu, W.; Cooper, E. I.; Angell, C. A. Ionic Liquids: Ion Mobilities, Glass Temperatures, and Fragilities. *J. Phys. Chem. B* **2003**, *107*, 6170−6178.
(73) Umebayashi, Y.; Yamaguchi, T.; Fukuda, S.; Mitsugi, T.; Takeuchi, M.; Fujii, K.; Ishiguro, S. Raman Spectroscopic Study on Alkaline Metal Ion Solvation in 1-Butyl-3-methylimidazolium Bis-(trifluoromethanesulfonyl)amide Ionic Liquid. *Anal. Sci.* **2008**, *24*, 1297−1304.
(74) Shirai, A.; Fujii, K.; Seki, S.; Umebayashi, Y.; Ishiguro, S.-I.; Ikeda, Y. Solvation of Lithium Ion in *N*,*N*-Diethyl-*N*-methyl-*N*-amide Using Raman and Multinuclear NMR Spectroscopy. *Anal. Sci.* **2008**, *24*, 1291−1296.